Contents lists available at ScienceDirect

Mechatronics

journal homepage: www.elsevier.com/locate/mechatronics

MIMO multirate feedforward controller design with selection of input multiplicities and intersample behavior analysis

Masahiro Mae *, Wataru Ohnishi, Hiroshi Fujimoto

The University of Tokyo, Japan

ARTICLE INFO

Keywords:
Feedforward control
Inverse system
Multirate
Multi-input/multi-output systems
Digital control
Position control

ABSTRACT

Inversion-based feedforward control is a basic method of tracking controls. The aim of this paper is to design MIMO multirate feedforward controller that improves continuous-time tracking performance in MIMO LTI systems considering not only on-sample but also intersample behavior. Several types of MIMO multirate feedforward controllers are designed and evaluated in terms of the 2-norm of the control inputs. The approach is compared with a conventional MIMO single-rate feedforward controller in simulations. The approach improves the intersample behavior through the optimal selection of input multiplicities with MIMO multirate system inversion.

1. Introduction

Inversion-based feedforward controllers are important in the tracking control of many high-precision mechatronic systems, such as wafer and LCD scanners, and industrial robots [1]. For the demands of high-performance, high-speed, and flexible tasks, many high-precision mechatronic systems have multiple degrees-of-freedom and are multi-input multi-output (MIMO) systems. Many high-precision mechatronic systems are typically controlled by single-input single-output (SISO) controllers under the assumption that they are mechanically decoupled, and coupling problems between axes can be disregarded. Several high-precision mechatronic systems with severe coupling problems between axes, such as a six-degree-of-freedom high-precision positioning stage, are controlled with MIMO controllers, such as SISO controllers with a continuous-time pre-compensator [2], the feedforward input shaping approach [3], and the feedforward H_∞ approach [4]. However, these continuous-time controllers are typically discretized by Tustin transform for digital implementation. Therefore, the effect of discretization by the zero-order hold is not strictly considered, and perfect tracking control cannot be achieved for a discrete-time nominal system.

In high-precision positioning systems with multiple actuators and sensors, such as a six-degree-of-freedom high-precision positioning stage, the number of actuators and sensors are typically imaginarily converted by coordinate transformation to the same number of degrees-of-freedom of motion [2]. In this framework, this paper mainly focuses on MIMO linear-time-invariant (LTI) systems with an equal number of inputs and outputs. For the tracking control of MIMO LTI systems, MIMO feedforward controllers must achieve good tracking performance by considering the coupling problems and redundancy of MIMO LTI systems.

Continuous-time stable inversion-based approaches such as those presented in [5–7] can be used in continuous-time systems. However, practical tracking controllers are often implemented by digital systems to afford flexibility and low cost [8]. Therefore, tracking control is conducted with digital control and presents some limitations owing to discretization. The main problem of the inversion-based feedforward controllers is the unstable discretized zeros, which are outside of the unit circle on the z-plane, of the controlled system discretized by a sampler and a holder. Inversion-based feedforward controllers are designed by the inverse of controlled systems, and they have unstable poles because of the unstable zeros of the controlled systems.

To overcome the discretized unstable zero problems, several approximated inverse approaches have been proposed for single-rate feedforward control, such as nonminimum-phase zeros ignore (NPZI) [9], zero-phase-error tracking control (ZPETC) [10] and zero-magnitude-error tracking controll (ZMETC) [11]. However, these approaches cannot achieve exact tracking on sampling points because of the approximation. An exact inverse approach, known as discrete-time stable inversion [12,13], has been presented; however, this approach cannot manage discretized zeros near $z = -1$ that become oscillating poles of the inversion-based feedforward controllers [14,15]. It is noteworthy that these single-rate feedforward control approaches can be extended to MIMO LTI systems [16,17]. FIR filter tuning with a gradient approximation-based algorithm is presented for decoupling control of MIMO systems using a discrete-time controller [18]. However, this

* Corresponding author.
E-mail address: mmae@ieee.org (M. Mae).

https://doi.org/10.1016/j.mechatronics.2020.102442
Received 2 February 2020; Received in revised form 2 September 2020; Accepted 13 September 2020

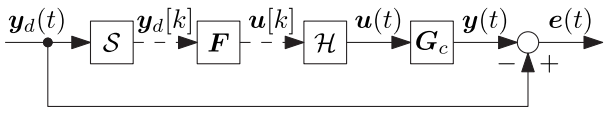

Fig. 1. Block diagram of tracking control. Continuous-time system G_c is controlled by discrete-time controller F with sampler $\mathcal{S}$ and holder $\mathcal{H}$. The objective is to minimize the continuous-time error $e(t)$.

approach uses an optimization in the algorithm and is not suitable when many types of references are used.

Based on these approaches used for single-rate feedforward control, a multirate control approach has been presented [19]. Compared with the single-rate system, the multirate system has all zeros at $z = 0$. Therefore, the multirate feedforward controller has all poles at $z = 0$; additionally, exact on-sample tracking can be achieved, and the intersample behavior is improved.

Previous studies have shown that the multirate feedforward control approach can be extended from the SISO LTI systems to the MIMO LTI systems [20]. The MIMO multirate feedforward controller is effective for rejecting cross-coupling effects compared with the basic pre-compensator approach [21]. The MIMO multirate feedforward controller can be designed as several types because of the redundancy of MIMO LTI systems and multirate sampling periods. In this paper, a procedure for designing an optimal MIMO multirate feedforward controller is presented.

The outline of this paper is as follows: In Section 2, the problem of tracking with digital control is formulated. In Section 3, the conventional MIMO single-rate feedforward control approach and its limitations are presented before the proposed approach is introduced. In Section 4, the proposed MIMO multirate feedforward control approach is presented. In Section 5, the advantages of the proposed approach are demonstrated via application to a MIMO motion system in the simulations. In Section 6, the conclusions of this study are presented.

2. Problem formulation

In this section, the control problem is formulated. The overview of the tracking control is shown in Fig. 1.

2.1. Definition of multi-input multi-output system

The state equation and the output equation of an m-input m-output nth-order continuous-time linear time-invariant system G_c are given by

$$\dot{\boldsymbol{x}}(t) = \boldsymbol{A}_c\boldsymbol{x}(t) + \boldsymbol{B}_c\boldsymbol{u}(t), \tag{1}$$

$$\boldsymbol{y}(t) = \boldsymbol{C}_c\boldsymbol{x}(t), \tag{2}$$

$$\boldsymbol{B}_c = \begin{bmatrix}\boldsymbol{b}_{c_1} & \cdots & \boldsymbol{b}_{c_m}\end{bmatrix}, \quad \boldsymbol{C}_c = \begin{bmatrix}\boldsymbol{c}_{c_1} & \cdots & \boldsymbol{c}_{c_m}\end{bmatrix}^{\mathsf{T}},$$

where the state variables are $\boldsymbol{x}(t) \in \mathbb{R}^{n\times 1}$, inputs are $\boldsymbol{u}(t) \in \mathbb{R}^{m\times 1}$, outputs are $\boldsymbol{y}(t) \in \mathbb{R}^{m\times 1}$, and the matrices are $\boldsymbol{A}_c \in \mathbb{R}^{n\times n}$, $\boldsymbol{B}_c \in \mathbb{R}^{n\times m}$, and $\boldsymbol{C}_c \in \mathbb{R}^{m\times n}$. This paper mainly focuses on MIMO LTI systems that have the same number of inputs and outputs. This is a natural assumption for mechatronic systems for achieving both state controllability and hardware cost reduction.

2.2. Discretization and sampling periods

Discrete-time system G_d discretized by the zero-order hold with G_c and the generalized sampling period δ is given by

$$\boldsymbol{x}[k+1] = \boldsymbol{A}_d\boldsymbol{x}[k] + \boldsymbol{B}_d\boldsymbol{u}[k], \tag{3}$$

$$\boldsymbol{y}[k] = \boldsymbol{C}_d\boldsymbol{x}[k], \tag{4}$$

where $k \in \mathbb{Z}$. $\boldsymbol{A}_d$, $\boldsymbol{B}_d$, and $\boldsymbol{C}_d$ are given by

$$\boldsymbol{A}_d = e^{\boldsymbol{A}_c\delta}, \quad \boldsymbol{B}_d = \int_0^\delta e^{\boldsymbol{A}_c\tau}\boldsymbol{B}_c\,\mathrm{d}\tau, \quad \boldsymbol{C}_d = \boldsymbol{C}_c. \tag{5}$$

In the discrete-time system, three sampling periods exist: T_r, T_y, and T_u, which represent the sampling periods of a reference $r(t)$, an output $y(t)$, and a control input $u(t)$, respectively. The three sampling periods T_r, T_y, and T_u are the same in the single-rate system but different in the multirate system.

2.3. Perfect tracking control and intersample behavior

In the tracking control problem, the discrete-time controller F should be designed as $G_dF = I$, where $G_d = \mathcal{S}G_c\mathcal{H}$, at every sampling point and achieves perfect tracking control.

The perfect tracking control is defined as follows [10]:

Definition 1. The perfect tracking control is defined as a method in which the plant output perfectly tracks the desired trajectory with zero tracking error at every sampling point.

It is important that the perfect tracking control only guarantees the tracking error on the discrete-time sampling points, but not in the continuous-time. In the tracking control problem, the objective is to minimize the continuous-time error $e(t)$. Therefore, not only on-sample tracking errors but also intersample tracking errors should be considered in the design of discrete-time controller F.

In this paper, two types of discrete-time controllers are presented, the first is a single-rate feedforward controller and the second is a multirate feedforward controller.

3. Single-rate feedforward control for multi-input multi-output system

Single-rate system G_s discretized by the zero-order hold with G_c and the sampling period $\delta = T_u$ is given by

$$\boldsymbol{x}[k+1] = \boldsymbol{A}_s\boldsymbol{x}[k] + \boldsymbol{B}_s\boldsymbol{u}[k], \tag{6}$$

$$\boldsymbol{y}[k] = \boldsymbol{C}_s\boldsymbol{x}[k]. \tag{7}$$

From the state space representation of single-rate system G_s, the control inputs $\boldsymbol{u}_{ff}[k]$ of single-rate feedforward controller F_{sr} for the reference of the desired output trajectory $\boldsymbol{r}[k] = \boldsymbol{y}_d[k+1]$ are given by

$$\boldsymbol{u}_{ff}[k] = \boldsymbol{F}_{sr}\boldsymbol{y}_d[k+1], \tag{8}$$

where F_{sr} is given by

$$\boldsymbol{F}_{sr} = \left[\begin{array}{c|c} \boldsymbol{A}_s - \boldsymbol{B}_s(\boldsymbol{C}_s\boldsymbol{B}_s)^{-1}\boldsymbol{C}_s\boldsymbol{A}_s & \boldsymbol{B}_s(\boldsymbol{C}_s\boldsymbol{B}_s)^{-1} \\ \hline -(\boldsymbol{C}_s\boldsymbol{B}_s)^{-1}\boldsymbol{C}_s\boldsymbol{A}_s & (\boldsymbol{C}_s\boldsymbol{B}_s)^{-1} \end{array}\right]. \tag{9}$$

There is exact tracking of the desired output trajectory $\boldsymbol{y}_d$ at every sample of T_u in the systems with the single-rate feedforward control.

However, the single-rate feedforward controller has a problem. It is known that a single-rate system discretized by the zero-order hold has discretized zeros depending on the relative order of the continuous-time system [22]. The discretized zeros appear around $z = -1$ on the real axis on the z-plane. The single-rate feedforward controller is designed as the inverse of the single-rate system, and the zeros of the single-rate system become the poles of the single-rate feedforward controller. When the pole of the system is near $z = -1$ of the z-plane, the system oscillates or diverges. Therefore, the single-rate feedforward controller has the problem that the generated control inputs may oscillates or diverges. If the single-rate feedforward controller F_{sr} has unstable poles, a stable inversion approach or an approximated inverse approach will be used, see details in [12,17].

On the other hand, the multirate feedforward controller is designed such that all poles are at $z = 0$ and the generated control inputs do not oscillate or diverge. In this paper, a MIMO multirate feedforward controller is proposed to render the continuous-time error smaller than that of a MIMO single-rate feedforward controller.

4. Multirate feedforward control for multi-input multi-output system

In this section, the design method of the MIMO multirate feedforward controller is proposed for the tracking control of MIMO LTI systems. The multirate feedforward control offers the advantage of intersample behavior compared with the single-rate feedforward control [13].

4.1. Design of input matrix from generalized controllability indices

The generalized controllability indices are defined as follows [20]:

Definition 2. The generalized controllability indices of $\boldsymbol{A}_c \in \mathbb{R}^{n\times n}$ and $\boldsymbol{B}_c = [\boldsymbol{b}_{c1}, \dots, \boldsymbol{b}_{cm}] \in \mathbb{R}^{n\times m}$ are defined as follows:

$$\{\boldsymbol{b}_{c1}, \dots, \boldsymbol{b}_{cm}, \boldsymbol{A}_c\boldsymbol{b}_{c1}, \dots, \boldsymbol{A}_c\boldsymbol{b}_{cm}, \dots, \boldsymbol{A}_c^{n-1}\boldsymbol{b}_{cm}\}.$$

If $(\boldsymbol{A}_c, \boldsymbol{B}_c)$ is a controllable pair, n linearly independent vectors can be selected from the generalized controllability indices.

The generalized controllability indices are the sets of input multiplicities σ_l.

The input multiplicities σ_l are defined as follows [20]:

Definition 3. Input multiplicities σ_l are defined as the number of the inputs originating from the same input in the same frame period T_f.

Setting φ as a set of n vectors selected from the generalized controllability indices, σ_l and N are defined as

$$\sigma_l = \text{number}\{k | \boldsymbol{A}_c^{k-1}\boldsymbol{b}_{cl} \in \varphi\}, \tag{10}$$

$$N = \max(\sigma_l), \tag{11}$$

where $l \in \mathbb{N}$ is the index of the inputs. The plant order n is equal to the sum of input multiplicities σ_l as

$$\sum_{l=1}^{m} \sigma_l = n. \tag{12}$$

In MIMO LTI systems, n vectors are selected from the generalized controllability indices, and the full row rank matrix $\boldsymbol{B}$ can be designed for almost all discretized sampling periods.[1] Therefore, several types of multirate systems are designed based on the selection of input multiplicities.

Based on the set of input multiplicities, T_{u_l}, which is the sampling period of lth input u_l, is defined as

$$T_{u_l} = \frac{N}{\sigma_l} T_u. \tag{13}$$

It is noteworthy that the sampling period T_u is the smallest value of T_{u_l}.

A sampling period T_f is defined as the frame period, which is the largest value among T_r, T_y, and T_u. In this study, the frame period T_f of the multirate system is defined as

$$T_f = T_r = NT_y = NT_u. \tag{14}$$

The multirate system $\boldsymbol{G}$ discretized by the zero-order hold with $\boldsymbol{G}_c$ and the sampling period $\delta = T_{u_l}$ is given by

$$\boldsymbol{x}[i+1] = \boldsymbol{A}\boldsymbol{x}[i] + \boldsymbol{B}\boldsymbol{u}[i], \tag{15}$$

$$\boldsymbol{y}[i] = \boldsymbol{C}\boldsymbol{x}[i], \tag{16}$$

where $i \in \mathbb{Z}$. $\boldsymbol{A}$, $\boldsymbol{B}$, $\boldsymbol{x}[i]$, and $\boldsymbol{u}[i]$ are given by

$$\boldsymbol{A} = e^{\boldsymbol{A}_c T_f}, \tag{17}$$

[1] This is possible because the controllability of a continuous-time system is not preserved in the discrete system only if the two poles η_i and η_j have the same real parts, and the discretizing sampling period T satisfies $\eta_i = \eta_j + j\frac{2k\pi}{T}$ $(k = \pm1, \pm2, \dots)$; furthermore, it is limited to only several cases [23].

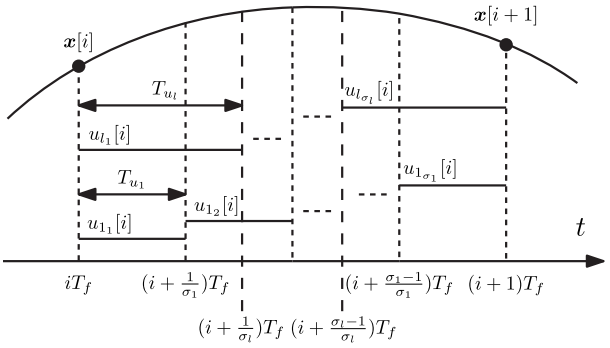

Fig. 2. MIMO multirate input control.

$$\boldsymbol{B} = \begin{bmatrix} \boldsymbol{B}_1 & \cdots & \boldsymbol{B}_l & \cdots & \boldsymbol{B}_m \end{bmatrix}, \tag{18}$$

$$\boldsymbol{C} = \boldsymbol{C}_c, \tag{19}$$

$$\boldsymbol{x}[i] = \boldsymbol{x}(iT_f), \tag{20}$$

$$\begin{aligned}\boldsymbol{u}[i] &= \begin{bmatrix}\boldsymbol{u}_1[i] & \cdots & \boldsymbol{u}_m[i]\end{bmatrix}^{\mathsf{T}} \\ &= \begin{bmatrix}u_{1_1}[i] & \cdots & u_{1_{\sigma_1}}[i] & u_{2_1}[i] & \cdots & u_{m_{\sigma_m}}[i]\end{bmatrix}^{\mathsf{T}},\end{aligned} \tag{21}$$

and $\boldsymbol{B}_l$, $\boldsymbol{A}_{s_l}$ and $\boldsymbol{b}_{s_l}$ are defined as

$$\boldsymbol{B}_l = \begin{bmatrix}\boldsymbol{A}_{s_l}^{\sigma_l-1}\boldsymbol{b}_{s_l} & \boldsymbol{A}_{s_l}^{\sigma_l-2}\boldsymbol{b}_{s_l} & \cdots & \boldsymbol{A}_{s_l}\boldsymbol{b}_{s_l} & \boldsymbol{b}_{s_l}\end{bmatrix}, \tag{22}$$

$$\boldsymbol{A}_{s_l} = e^{\boldsymbol{A}_c T_{u_l}}, \quad \boldsymbol{b}_{s_l} = \int_0^{T_{u_l}} e^{\boldsymbol{A}_c \tau}\boldsymbol{b}_{c_l}\,\mathrm{d}\tau. \tag{23}$$

The input matrix $\boldsymbol{B}$ in a multirate system is designed by the generalized controllability indices based on the set of input multiplicities σ_l. It becomes a nonsingular square matrix because of the definition of the generalized controllability indices. The states and inputs of the multirate system are shown in Fig. 2.

4.2. Controller design and control input generation

From the state equation of the multirate system (15), the control inputs $\boldsymbol{u}_{ff}[i]$ of the multirate feedforward controller $\boldsymbol{F}_{mr}$ for the reference of the desired state trajectory $\boldsymbol{r}[i] = \boldsymbol{x}_d[i+1]$ are given by

$$\boldsymbol{u}_{ff}[i] = \boldsymbol{F}_{mr}\boldsymbol{x}_d[i+1], \tag{24}$$

where $\boldsymbol{F}_{mr}$ and z are given by

$$\begin{aligned}\boldsymbol{F}_{mr} &= \boldsymbol{B}^{-1}(\boldsymbol{I} - z^{-1}\boldsymbol{A}) \\ &= \left[\begin{array}{c|c} \boldsymbol{O} & \boldsymbol{I} \\ \hline -\boldsymbol{B}^{-1}\boldsymbol{A} & \boldsymbol{B}^{-1}\end{array}\right],\end{aligned} \tag{25}$$

$$z = e^{sT_f}. \tag{26}$$

There is exact tracking of the desired state trajectory $\boldsymbol{x}_d$ at every N samples of T_u in the nominal system with the multirate feedforward control. It is noteworthy that all poles of multirate feedforward controller $\boldsymbol{F}_{mr}$ are $z = 0$ because the state matrix of $\boldsymbol{F}_{mr}$ is $\boldsymbol{O}$, and a smooth control input is generated compared with single-rate feedforward controller $\boldsymbol{F}_{sr}$. For details regarding the desired state trajectory generation, see [24,25]. A block diagram of the control system is shown in Fig. 3. L is a discrete-time lifting operator [8]. L^{-1} outputs the elements of the Nth dimensional vector $\boldsymbol{u}_{ff}[i]$, which are inputs at every period T_f, in the order from 1 to σ_l by T_{u_l}.

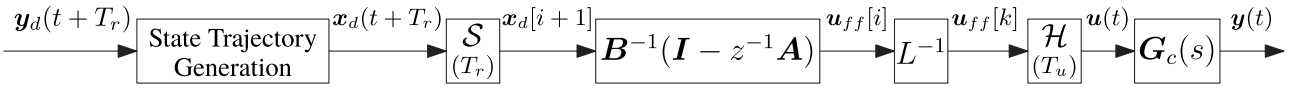

Fig. 3. Block diagram of MIMO multirate feedforward control. S, $\mathcal{H}$, L, and z denote sampler, holder, lifting operator [8], and e^{sT_f}, respectively.

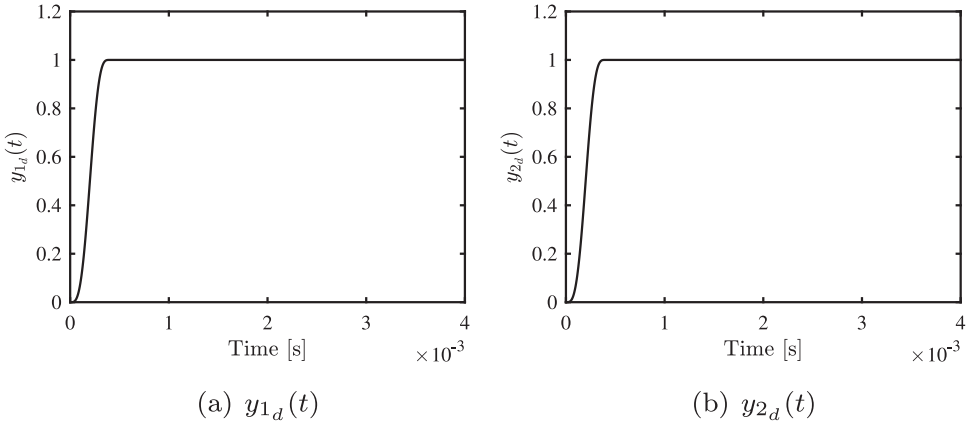

Fig. 4. Desired output trajectory $\boldsymbol{y}_d(t) = [y_{1_d}(t)\ y_{2_d}(t)]^{\mathrm{T}}$: they are 7th-order polynomials, respectively.

4.3. Optimal selection of input multiplicities

Several types of multirate feedforward controllers can be designed based on multirate system $\boldsymbol{G}$ with the selection of input multiplicities σ_l. There is exact tracking of the desired state trajectory $\boldsymbol{x}_d$ at every N samples of T_u in the systems with all types of multirate feedforward controllers [21]. However, the control inputs and intersample behavior differ depending on the multirate system $\boldsymbol{G}$. For the application of high-precision positioning control in mechatronic systems, the continuous-time tracking error is preferred to be small, and the control input $\boldsymbol{u}$ should be smaller because of the limitation of mechatronic systems. An approach for designing the optimal MIMO multirate feedforward controller to reduce the 2-norm of control inputs is proposed in the remaining of this section.

From the state equation of a multirate system (15), the part in which the control input $\boldsymbol{u}$ affects the state $\boldsymbol{x}$ is given by

$$\boldsymbol{B}\boldsymbol{u}[i] = \boldsymbol{x}[i+1] - \boldsymbol{A}\boldsymbol{x}[i]. \tag{27}$$

In the multirate feedforward control, there is exact tracking of the states $\boldsymbol{x}[i]$ and $\boldsymbol{x}[i+1]$. $\boldsymbol{v}[i]$, which is the difference of the states, is defined as

$$\boldsymbol{v}[i] = \boldsymbol{x}[i+1] - \boldsymbol{A}\boldsymbol{x}[i], \tag{28}$$

and the control input $\boldsymbol{u}[i]$ is given by

$$\boldsymbol{u}[i] = \boldsymbol{B}^{-1}\boldsymbol{v}[i]. \tag{29}$$

The square of the 2-norm of the control input $\|\boldsymbol{u}[i]\|_2^2 = u_1^2 + \cdots + u_n^2$ is given by

$$\|\boldsymbol{u}[i]\|_2^2 = \boldsymbol{v}^{\mathrm{T}}[i](\boldsymbol{B}^{-1})^{\mathrm{T}}\boldsymbol{B}^{-1}\boldsymbol{v}[i], \tag{30}$$

and $\|\boldsymbol{u}[i]\|_2^2$ becomes a quadratic form of $\boldsymbol{v}[i]$.

For the normalization of the difference of the states, $\boldsymbol{v}[i]$ is defined as a unit sphere as follows:

$$\|\boldsymbol{v}[i]\|_2^2 = v_1^2 + \cdots + v_n^2 = 1. \tag{31}$$

Based on the relationship between the range of a quadratic form with a unit sphere and eigenvalues [26], the range of $\|\boldsymbol{u}[i]\|_2^2$ is given by

$$\lambda_n \le \|\boldsymbol{u}[i]\|_2^2 \le \lambda_1 \quad (\lambda_n \le \lambda_{(n-1)} \le \cdots \le \lambda_1), \tag{32}$$

where λ_i is the eigenvalue of $(\boldsymbol{B}^{-1})^{\mathrm{T}}\boldsymbol{B}^{-1}$. λ_{ci}, which is the eigenvalue of $\boldsymbol{B}\boldsymbol{B}^{\mathrm{T}}$, is the reciprocal of λ_i defined as follows:

$$\lambda_{ci} = \frac{1}{\lambda_i}, \tag{33}$$

and the range of $\|\boldsymbol{u}[i]\|_2^2$ given by

$$\frac{1}{\lambda_{cn}} \le \|\boldsymbol{u}[i]\|_2^2 \le \frac{1}{\lambda_{c1}} \quad (\lambda_{c1} \le \lambda_{c2} \le \cdots \le \lambda_{cn}). \tag{34}$$

σ_{ci}, which is the singular value of the input matrix $\boldsymbol{B}$, is the square root of λ_{ci} defined as follows:

$$\sigma_{ci}(\boldsymbol{B}) = \sqrt{\lambda_{ci}(\boldsymbol{B}\boldsymbol{B}^{\mathrm{T}})}. \tag{35}$$

The range of the 2-norm of the control input $\|\boldsymbol{u}[i]\|_2$ is given by

$$\frac{1}{\sigma_{cn}} \le \|\boldsymbol{u}[i]\|_2 \le \frac{1}{\sigma_{c1}} \quad (\sigma_{c1} \le \sigma_{c2} \le \cdots \le \sigma_{cn}). \tag{36}$$

If the 2-norm of the control input $\|\boldsymbol{u}[i]\|_2$ is extremely large, then it is not suitable for mechatronic systems owing to their limitations. The upper bound of the 2-norm of the control input $\|\boldsymbol{u}[i]\|_2$ is smaller, rendering the smallest singular value $\sigma_{c1}(\boldsymbol{B})$ larger. Hence, the input multiplicity is selected such that the smallest singular value $\sigma_{c1}(\boldsymbol{B})$ becomes the largest. Therefore, the optimal design of the MIMO multirate feedforward controller for achieving the maximum value of the 2-norm of the control inputs smaller is proposed. The MIMO multirate feedforward controller cannot specify the band of the continuous-time error because it only guarantees the exact tracking of the desired state trajectory $\boldsymbol{x}_d$ at every frame period T_f in the nominal system; however, the intersample behavior becomes smoothly connected between the discrete sampling points in continuous time with the control inputs of the optimally designed controller. The analysis of the bound of the continuous-time error is an open issue.

4.4. Example: intersample behavior of multirate feedforward in different sets of input multiplicities

In this study, the optimal design of the MIMO multirate feedforward controller is validated using a numerical simulation example.

Continuous-time system $\boldsymbol{G}_c$ is defined as a transfer function matrix (37) (see Box I). The reference of the desired output trajectory $\boldsymbol{y}_d$ is given by 7th-order polynomial, which changes from 0 to 1 in 0 s to 400 μs for each output as shown in Fig. 4. The sampling period of the

$$\boldsymbol{G}_c(s) = \frac{1}{s^6 + 8895s^5 + 3.979\times10^7 s^4 + 2.428\times10^9 s^3 + 9.099\times10^{12} s^2 + 4.382\times10^{13} s + 24} \begin{bmatrix} 4.702\times10^{10}s^2 + 2.294\times10^{11}s + 5.477\times10^{15} & 1.387\times10^8 s^2 + 1.233\times10^{12}s + 5.477\times10^{15} \\ 5.477\times10^{15} & 1220s^4 + 1.085\times10^7 s^3 + 4.835\times10^{10}s^2 + 1.462\times10^{12}s + 5.477\times10^{15} \end{bmatrix} \tag{37}$$

Box I.

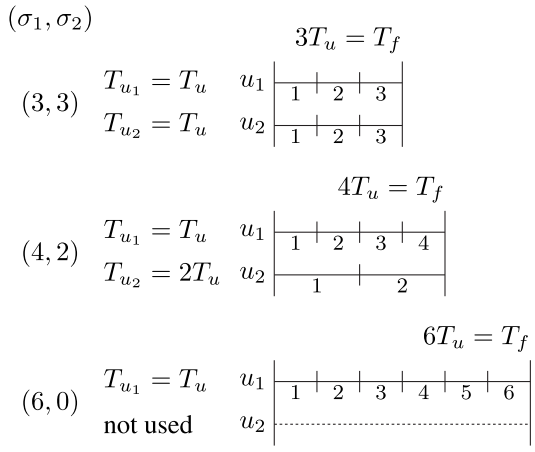

Fig. 5. Examples of multirate inputs. Two inputs u_1 and u_2 are generated based on the set of input multiplicities (σ_1, σ_2). Control inputs with 0 input multiplicity are not used.

control input is set to $T_u = 400\,\mu s$. For the design of the MIMO multirate feedforward controller, seven types of the sets of input multiplicities are selected as follows:

$$(\sigma_1, \sigma_2) = (0,6), (1,5), (2,4), (3,3), (4,2), (5,1), (6,0). \tag{38}$$

The examples of multirate inputs are shown in Fig. 5.

The smallest singular value $\sigma_{c1}(\boldsymbol{B})$ and the simulation results are shown in Table 1. Based on the procedure for designing the optimal MIMO multirate feedforward controller, the set of input multiplicities in which the smallest singular value $\sigma_{c1}(\boldsymbol{B})$ is the largest is the optimal set of input multiplicities for the controlled system. The advantage of the proposed approach is that the optimal MIMO multirate feedforward controller can be designed without numerical simulations. When the order of the system is high or the number of inputs and outputs is large, the number of the sets of input multiplicities becomes enormous. Therefore, testing all sets with several references in numerical simulations requires a significant amount of time, for which the proposed design procedure is effective.

The validity of the proposed design procedure can be confirmed from the root mean square and the maximum absolute value of control inputs $\boldsymbol{u}$ and tracking errors $\boldsymbol{e}$ in Table 1. The trend is that control inputs $\boldsymbol{u}$ and tracking errors $\boldsymbol{e}$ decrease when the smallest singular value $\sigma_{c1}(\boldsymbol{B})$ is large. Based on Table 1, the optimal MIMO multirate feedforward controller is designed with the set of input multiplicities $(\sigma_1, \sigma_2) = (4,2)$, which renders the smallest singular value $\sigma_{c1}(\boldsymbol{B})$ the largest, and the root mean square of the tracking errors $\boldsymbol{e}$ are the smallest in all sets.

In summary, the proposed design procedure is validated, and the optimal MIMO multirate feedforward controller can be designed with the set of input multiplicities, which renders the smallest singular value $\sigma_{c1}(\boldsymbol{B})$ the largest without incurring a significant amount of time on numerical simulations.

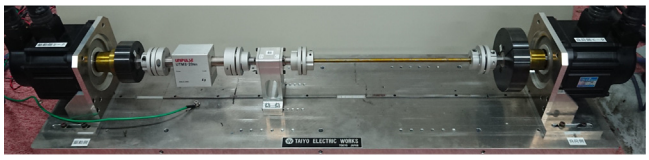

(a) Photograph of two-inertia system motor bench.

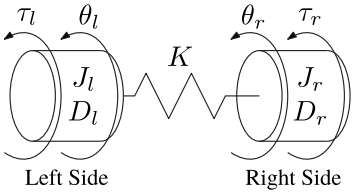

(b) Model of two-inertia system.

Fig. 6. Details of two-inertia system motor bench. In this study, the two-inertia system motor bench is modeled as a two-input two-output system. The two inputs are left side torque τ_l and right side torque τ_r. The two outputs are left side angle θ_l and right side angle θ_r.

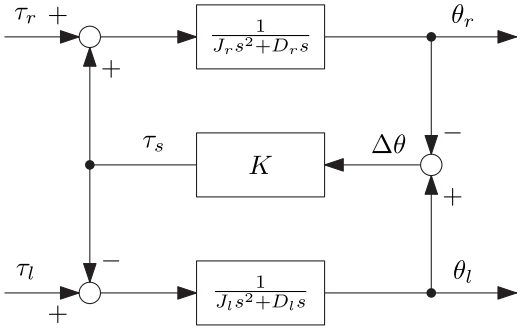

Fig. 7. Block diagram of two-inertia system.

5. Verification in multi-input multi-output positioning system

The tracking performance considering the intersample behavior of the optimal MIMO multirate feedforward controller is verified and compared with that of a MIMO single-rate feedforward controller.

5.1. System modeling

The approach is validated on a two-inertia system motor bench, as shown in Fig. 6(a). The two-inertia system motor bench comprises two motors on the left and right sides, and the two motors are connected by a flexible shaft, as shown in Fig. 6(b). The two-inertia system motor bench is used for theoretical and applicability validation. It comprises an 20 bit/rev optical encoder on both sides, which offers a sufficiently high resolution for high-precision mechatronic systems. In this study, the two-inertia system motor bench is modeled as a two-input two-output 4th-order system. The block diagram of the system is shown

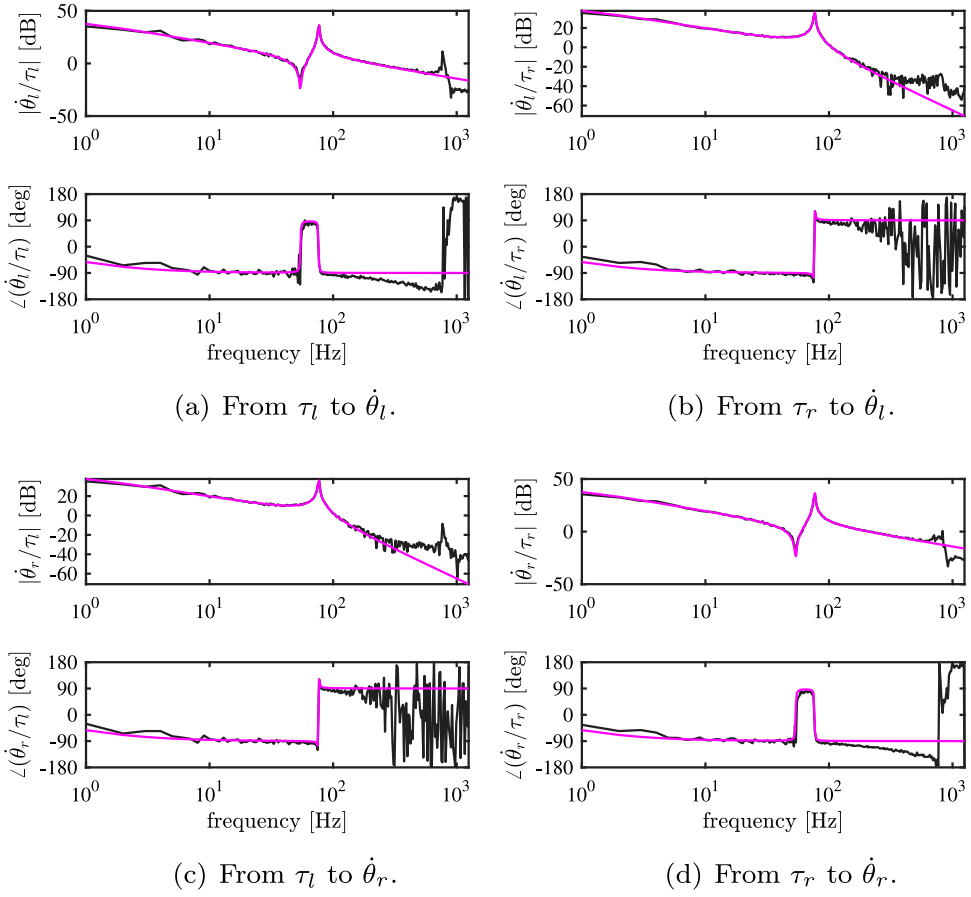

Fig. 8. Bode diagram of two-inertia system motor bench. Black line indicates frequency response function measurement of the system; magenta line indicates identified continuous-time system.

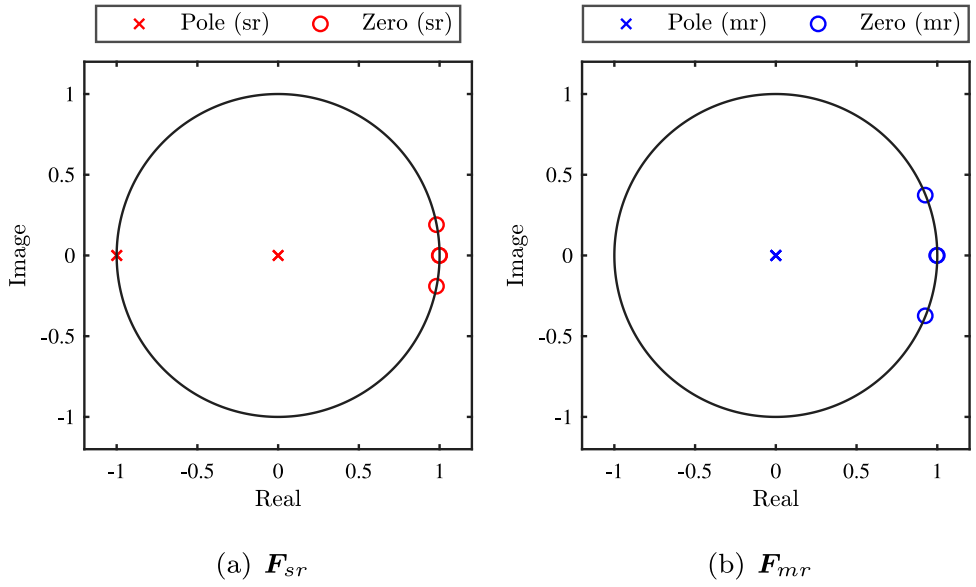

Fig. 9. Poles and zeros of multirate feedforward controller $\boldsymbol{F}_{mr}$ and single-rate feedforward controller $\boldsymbol{F}_{sr}$ with unit circle on z-plane.

Table 1
$\sigma_{c1}(\boldsymbol{B})$, the smallest singular value of $\boldsymbol{B}$, and root mean square and maximum absolute value of control inputs $\boldsymbol{u}$ and tracking errors $\boldsymbol{e}$ based on the sets of input multiplicities (σ_1, σ_2).

(σ_1, σ_2)	$\sigma_{c1}(\boldsymbol{B})$	RMS(u_1)	MAX($\lvert u_1 \rvert$)	RMS(u_2)	MAX($\lvert u_2 \rvert$)	RMS(e_1)	MAX($\lvert e_1 \rvert$)	RMS(e_2)	MAX($\lvert e_2 \rvert$)
(0, 6)	1.86×10^{-16}	0.00×10^{00}	0.00×10^{00}	9.81×10^{04}	2.27×10^{05}	4.48×10^{-01}	9.94×10^{-01}	7.34×10^{00}	1.53×10^{01}
(1, 5)	6.77×10^{-13}	5.54×10^{-12}	7.83×10^{-12}	1.71×10^{05}	4.27×10^{05}	4.01×10^{-01}	9.88×10^{-01}	9.30×10^{00}	2.47×10^{01}
(2, 4)	8.09×10^{-07}	2.24×10^{-10}	5.01×10^{-10}	3.95×10^{05}	8.37×10^{05}	3.28×10^{-01}	9.70×10^{-01}	1.40×10^{01}	3.67×10^{01}
(3, 3)	4.70×10^{-07}	4.70×10^{03}	1.48×10^{04}	6.72×10^{05}	1.73×10^{06}	2.26×10^{-01}	8.50×10^{-01}	4.01×10^{01}	1.28×10^{02}
(4, 2)	1.54×10^{-04}	2.06×10^{03}	4.78×10^{03}	8.12×10^{02}	1.29×10^{03}	2.77×10^{-01}	9.20×10^{-01}	3.09×10^{-01}	8.99×10^{-01}
(5, 1)	5.70×10^{-07}	5.84×10^{05}	1.51×10^{06}	2.27×10^{03}	3.21×10^{03}	3.44×10^{01}	1.01×10^{02}	7.66×10^{-01}	1.70×10^{00}
(6, 0)	1.01×10^{-06}	3.44×10^{05}	7.45×10^{05}	0.00×10^{00}	0.00×10^{00}	1.05×10^{01}	2.58×10^{01}	4.11×10^{-01}	9.96×10^{-01}

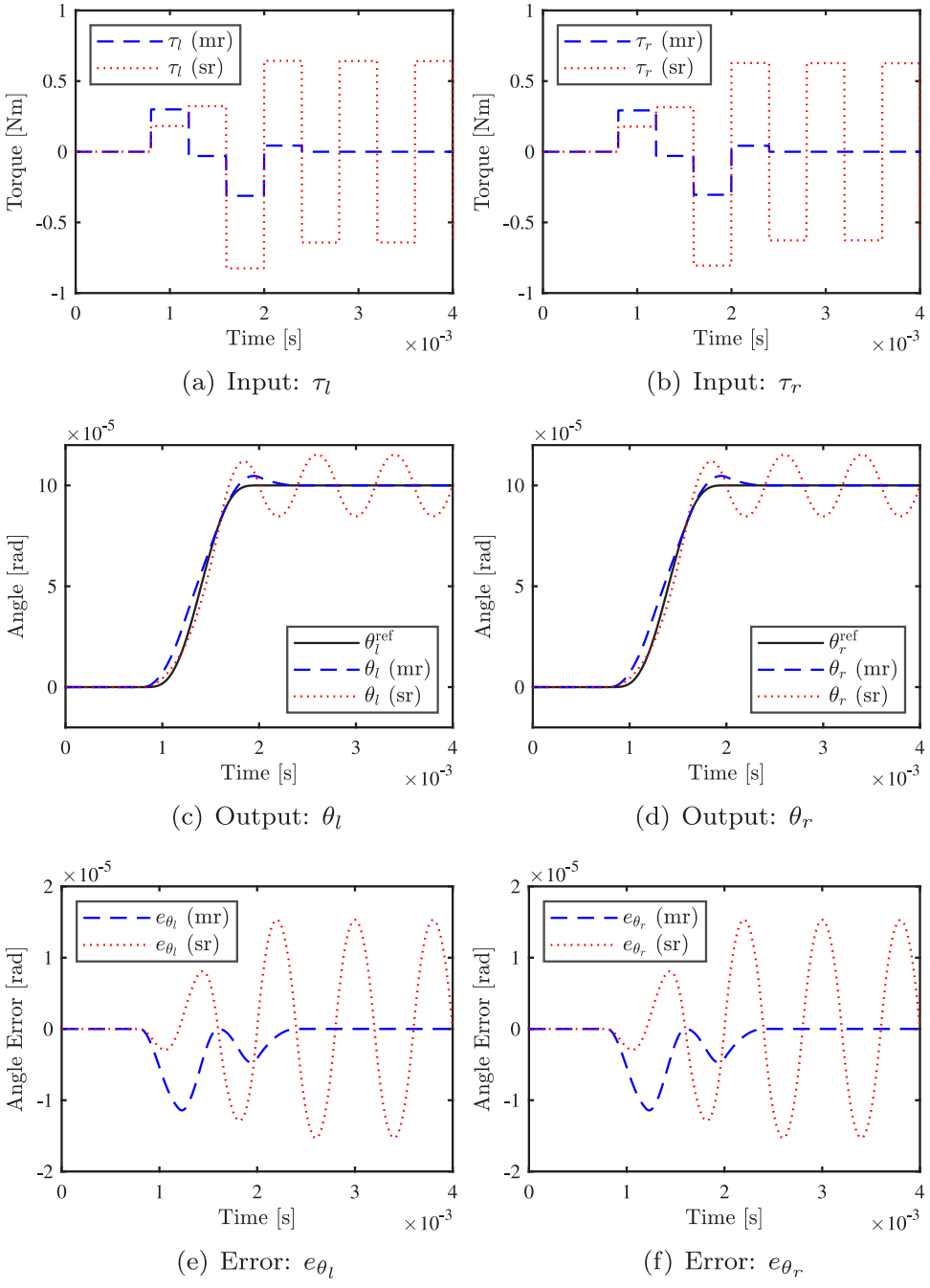

(a) Input: τ_l (b) Input: τ_r

(c) Output: θ_l (d) Output: θ_r

(e) Error: e_{θ_l} (f) Error: e_{θ_r}

Fig. 10. Simulation results of multirate and single-rate feedforward control.

in Fig. 7. The two inputs $\boldsymbol{u}$ are left and right side torques, τ_l and τ_r, respectively, and the outputs $\boldsymbol{y}$ are left and right side angles, θ_l and θ_r, respectively. The Bode diagram of the frequency response function measurement of the system is shown in Fig. 8. The measurement is performed in an identification experiment with a multisine input [27] from 1 Hz to 1249 Hz, and a sampling frequency of 2.5 kHz. Based on the

Table 2
Parameters of two-inertia system motor bench.

J_l	8.40×10^{-4} kg m^2	J_r	8.20×10^{-4} kg m^2
D_l	4.00×10^{-3} N m s/rad	D_r	4.00×10^{-3} N m s/rad
K	95.5 N m/rad		

frequency response function measurement, the parameters of the two-inertia system motor bench are shown in Table 2, and the identified continuous-time system $\boldsymbol{G}_c$ is given by the state space model with the state equation (39) and the output equation (40).

$$\frac{\mathrm{d}}{\mathrm{d}t}\begin{bmatrix}\theta_l(t)\\ \dot{\theta}_l(t)\\ \theta_r(t)\\ \dot{\theta}_r(t)\end{bmatrix} = \begin{bmatrix}0 & 1 & 0 & 0\\ -\frac{K}{J_l} & -\frac{D_l}{J_l} & \frac{K}{J_l} & 0\\ 0 & 0 & 0 & 1\\ \frac{K}{J_r} & 0 & -\frac{K}{J_r} & -\frac{D_r}{J_r}\end{bmatrix}\begin{bmatrix}\theta_l(t)\\ \dot{\theta}_l(t)\\ \theta_r(t)\\ \dot{\theta}_r(t)\end{bmatrix} + \begin{bmatrix}0 & 0\\ \frac{1}{J_l} & 0\\ 0 & 0\\ 0 & \frac{1}{J_r}\end{bmatrix}\begin{bmatrix}\tau_l(t)\\ \tau_r(t)\end{bmatrix} \tag{39}$$

$$\begin{bmatrix}\theta_l(t)\\ \theta_r(t)\end{bmatrix} = \begin{bmatrix}1 & 0 & 0 & 0\\ 0 & 0 & 1 & 0\end{bmatrix}\begin{bmatrix}\theta_l(t)\\ \dot{\theta}_l(t)\\ \theta_r(t)\\ \dot{\theta}_r(t)\end{bmatrix} \tag{40}$$

5.2. Conditions

The conventional MIMO single-rate feedforward controller $\boldsymbol{F}_{sr}$ and the proposed MIMO multirate feedforward controller $\boldsymbol{F}_{mr}$ are compared in the tracking control of continuous-time system $\boldsymbol{G}_c$. Based on the proposed approach, the optimal MIMO multirate feedforward controller is designed for $\boldsymbol{G}_c$ with the set of input multiplicities $(\sigma_1, \sigma_2) = (2, 2)$, which renders the smallest singular value $\sigma_{c1}(\boldsymbol{B})$ the largest. The poles and zeros of feedforward controllers $\boldsymbol{F}_{sr}$ and $\boldsymbol{F}_{mr}$ are shown in Fig. 9. As shown in Fig. 9(a), the conventional MIMO single-rate feedforward controller $\boldsymbol{F}_{sr}$ has one pole near $z = -1$, resulting in oscillation. As shown in Fig. 9(b), the proposed MIMO multirate feedforward controller $\boldsymbol{F}_{mr}$ has all poles on $z = 0$. The reference of the desired output trajectory $\boldsymbol{y}_d$ is given by 7th-order polynomial, which changes from 0 to 100 μrad in 0.8 ms to 2 ms for each output. The sampling period of the control input is set to $T_u = 400$ μs. From these conditions, the reference signal is sufficiently steep enough compared with T_u.

5.3. Results: intersample behavior of multirate feedforward and single-rate feedforward

The simulation results are shown in Fig. 10. Fig. 10(a) and Fig. 10(b) show that the control inputs of the conventional MIMO single-rate feedforward controller $\boldsymbol{F}_{sr}$ oscillate, whereas the proposed MIMO multirate feedforward controller $\boldsymbol{F}_{mr}$ generates the smooth control inputs. Fig. 10(c) and Fig. 10(d) show that the outputs of the single-rate feedforward controller oscillate because of the oscillating control inputs, whereas the outputs of the multirate feedforward controller stabilize after 2.4 ms. Fig. 10(e) and Fig. 10(f) show that the continuous-time tracking error of the multirate feedforward controller is smaller than that of the single-rate feedforward controller, thereby validating the effectiveness of the proposed approach.

A MIMO multirate feedforward controller is used in the two-degree-of-freedom robust control with feedback controllers which reduce modeling error and disturbances. The role of the feedforward controller is the nominal tracking performance in the two-degree-of-freedom control scheme, and the simulation validations accurately verify it. In summary, the proposed optimal MIMO multirate feedforward controller outperforms the conventional MIMO single-rate feedforward controller by yielding smooth control inputs and fewer continuous-time tracking errors.

6. Conclusion

A procedure of an optimal MIMO multirate feedforward controller design is proposed. The optimal MIMO multirate feedforward controller renders the upper bound of the 2-norm of the control input $\|\boldsymbol{u}[i]\|_2$ smaller; consequently, the continuous-time tracking errors reduce. A numerical simulation is conducted for a 6th-order system, and the proposed design procedure for the selection of input multiplicities is validated.

The continuous-time tracking errors of the proposed MIMO multirate feedforward controller $\boldsymbol{F}_{mr}$ are compared with those of the conventional MIMO single-rate feedforward controller $\boldsymbol{F}_{sr}$ using a two-inertia system motor bench. Depending on the poles of each controller, the conventional single-rate controller generates oscillated control inputs, whereas the proposed multirate controller generated smooth control inputs. Consequently, the continuous-time tracking errors of the multirate controller are fewer than those of the single-rate controller in the MIMO LTI system.

Ongoing research focuses on MIMO LTI systems that have a different number of inputs and outputs, and a combination of single-rate and multirate controllers.

Declaration of competing interest

The authors declare that they have no known competing financial interests or personal relationships that could have appeared to influence the work reported in this paper.

References

[1] Oomen T. Advanced motion control for precision mechatronics: Control, identification, and learning of complex systems. IEEJ J Ind Appl 2018;7(2):127–40. http://dx.doi.org/10.1541/ieejjia.7.127.

[2] Butler H. Position control in lithographic equipment [applications of control]. IEEE Control Syst 2011;31(5):28–47. http://dx.doi.org/10.1109/MCS.2011.941882.

[3] Al Hamidi Y, Rakotondrabe M. Multi-mode vibration suppression in MIMO systems by extending the zero placement input shaping technique: Applications to a 3-DOF piezoelectric tube actuator. Actuators 2016;5(2):13. http://dx.doi.org/10.3390/act5020013.

[4] Habineza D, Zouari M, Le Gorrec Y, Rakotondrabe M. Multivariable compensation of hysteresis, creep, badly damped vibration, and cross couplings in multiaxes piezoelectric actuators. IEEE Trans Autom Sci Eng 2018;15(4):1639–53. http://dx.doi.org/10.1109/TASE.2017.2772221.

[5] Hunt L, Meyer G, Su R. Noncausal inverses for linear systems. IEEE Trans Automat Control 1996;41(4):608–11. http://dx.doi.org/10.1109/9.489285.

[6] Devasia S, Chen D, Paden B. Nonlinear inversion-based output tracking. IEEE Trans Automat Control 1996;41(7):930–42. http://dx.doi.org/10.1109/9.508898.

[7] Sogo T. On the equivalence between stable inversion for nonminimum phase systems and reciprocal transfer functions defined by the two-sided Laplace transform. Automatica 2010;46(1):122–6. http://dx.doi.org/10.1016/j.automatica.2009.10.008.

[8] Chen T, Francis BA. Optimal sampled-data control systems. London: Springer London; 1995, http://dx.doi.org/10.1007/978-1-4471-3037-6, arXiv:1011.1669v3.

[9] Butterworth J, Pao L, Abramovitch D. Analysis and comparison of three discrete-time feedforward model-inverse control techniques for nonminimum-phase systems. Mechatronics 2012;22(5):577–87. http://dx.doi.org/10.1016/j.mechatronics.2011.12.006.

[10] Tomizuka M. Zero phase error tracking algorithm for digital control. J Dyn Syst Meas Control 1987;109(1):65. http://dx.doi.org/10.1115/1.3143822.

[11] Wen J, Potsaid B. An experimental study of a high performance motion control system. In: Proceedings of the 2004 American control conference, vol. 6. IEEE; 2004, p. 5158–63. http://dx.doi.org/10.23919/ACC.2004.1384671.

[12] van Zundert J, Oomen T. On inversion-based approaches for feedforward and ILC. Mechatronics 2018;50(November 2016):282–91. http://dx.doi.org/10.1016/j.mechatronics.2017.09.010.

[13] Van Zundert J, Ohnishi W, Fujimoto H, Oomen T. Improving intersample behavior in discrete-time system inversion: With application to LTI and LPTV systems. IEEE/ASME Trans Mechatronics 2019;PP(c):1. http://dx.doi.org/10.1109/TMECH.2019.2953829.

[14] Moore KL, Bhattacharyya S, Dahleh M. Capabilities and limitations of multirate control schemes. Automatica 1993;29(4):941–51. http://dx.doi.org/10.1016/0005-1098(93)90098-E.

[15] Sogo T, Joo M. Design of compensators to relocate sampling zeros of digital control systems for DC motors. SICE J Control Meas Syst Integr 2012;5(5):283–9. http://dx.doi.org/10.9746/jcmsi.5.283.
[16] George K, Verhaegen M, Scherpen JMa. Stable inversion of MIMO linear discrete time non-minimum phase systems. In: Proceedings of the 7th Mediterranean Conference on Control and Automation. 1999. p. 267–81.
[17] Blanken L, Oomen T. Multivariable iterative learning control design procedures: From decentralized to centralized, illustrated on an industrial printer. IEEE Trans Control Syst Technol 2019;1–8. http://dx.doi.org/10.1109/TCST.2019.2903021, arXiv:1806.08550.
[18] Heertjes M, Hennekens D, Steinbuch M. MIMO feed-forward design in wafer scanners using a gradient approximation-based algorithm. Control Eng Pract 2010;18(5):495–506. http://dx.doi.org/10.1016/j.conengprac.2010.01.006.
[19] Fujimoto H, Hori Y, Kawamura A. Perfect tracking control based on multirate feedforward control with generalized sampling periods. IEEE Trans Ind Electron 2001;48(3):636–44. http://dx.doi.org/10.1109/41.925591.
[20] Fujimoto H. General framework of multirate sampling control and applications to motion control systems [Doctoral dissertation], 2000.
[21] Mae M, Ohnishi W, Fujimoto H, Hori Y. Perfect tracking control considering generalized controllability indices and application for high-precision stage in translation and pitching. IEEJ J Ind Appl 2019;8(2):263–70. http://dx.doi.org/10.1541/ieejjia.8.263.
[22] Åström K, Hagander P, Sternby J. Zeros of sampled systems. Automatica 1984;20(1):31–8. http://dx.doi.org/10.1016/0005-1098(84)90062-1.
[23] Kalman R. On the general theory of control systems. IFAC Proc Vol 1960;1(1):491–502. http://dx.doi.org/10.1016/S1474-6670(17)70094-8.
[24] Ohnishi W, Beauduin T, Fujimoto H. Preactuated multirate feedforward control for independent stable inversion of unstable intrinsic and discretization zeros. IEEE/ASME Trans Mechatronics 2019;24(2):863–71. http://dx.doi.org/10.1109/TMECH.2019.2896237.
[25] Mae M, Ohnishi W, Fujimoto H. State trajectory generation for MIMO multirate feedforward using singular value decomposition and time axis reversal. In: 2019 American control conference. IEEE; 2019, p. 5693–8. http://dx.doi.org/10.23919/ACC.2019.8815067.
[26] Lang S. Linear algebra. third ed. Springer; 1987.
[27] Pintelon R, Guillaume P, Rolain Y, Schoukens J, Van Hamme H. Parametric identification of transfer functions in the frequency domain-a survey. IEEE Trans Automat Control 1994;39(11):2245–60. http://dx.doi.org/10.1109/9.333769.

Masahiro Mae received the B.E. and M.S. degrees from the University of Tokyo in 2018 and 2020, respectively. He is currently pursuing the Ph.D. degree at the Department of Electrical Engineering and Information Systems, Graduate School of Engineering, the University of Tokyo. His research interests are in control engineering, precision motion control, multirate control, and multi-input multi-output systems. He is a student member of the Institute of Electrical and Electronics Engineers, the Institute of Electrical Engineers of Japan, and the Society of Instrumental and Control Engineers.

Wataru Ohnishi received the B.E., M.S., and Ph.D. degrees from the University of Tokyo, Japan in 2013, 2015, and 2018, respectively. Presently, he is an assistant professor with the Department of Electrical Engineering and Information Systems, Graduate School of Engineering, the University of Tokyo. His research interest includes high-precision motion control. He is a member of the Institute of Electrical and Electronics Engineers and the Institute of Electrical Engineers of Japan.

Hiroshi Fujimoto received the Ph.D. degree in the Department of Electrical Engineering from the University of Tokyo in 2001. In 2001, he joined the Department of Electrical Engineering, Nagaoka University of Technology, Niigata, Japan, as a research associate. From 2002 to 2003, he was a visiting scholar in the School of Mechanical Engineering, Purdue University, U.S.A. In 2004, he joined the Department of Electrical and Computer Engineering, Yokohama National University, Yokohama, Japan, as a lecturer and then became an associate professor in 2005. He has been an associate professor at the University of Tokyo since 2010. He received the Best Paper Awards from the IEEE Transactions on Industrial Electronics in 2001 and 2013, Isao Takahashi Power Electronics Award in 2010, Best Author Prize of SICE in 2010, the Nagamori Grand Award in 2016, and First Prize Paper Award IEEE Transactions on Power Electronics in 2016.

His interests are in control engineering, motion control, nano-scale servo systems, electric vehicle control, motor drive, visual servoing, and wireless motors. He is a senior member of IEE of Japan and IEEE. He is also a member of the Society of Instrument and Control Engineers, the Robotics Society of Japan, and the Society of Automotive Engineers of Japan.

He is an associate editor of IEEE/ASME Transactions on Mechatronics from 2010 to 2014, IEEE Industrial Electronics Magazine from 2006, IEE of Japan Transactions on Industrial Application from 2013, and Transactions on SICE from 2013 to 2016. He is a chairperson of the JSAE vehicle electrification committee from 2014 and a past chairperson of the IEEE/IES Technical Committee on Motion Control from 2012 to 2013.